Cell Reports

Real-Time In-Cell NMR Reveals the Intracellular Modulation of GTP-Bound Levels of RAS

Graphical Abstract

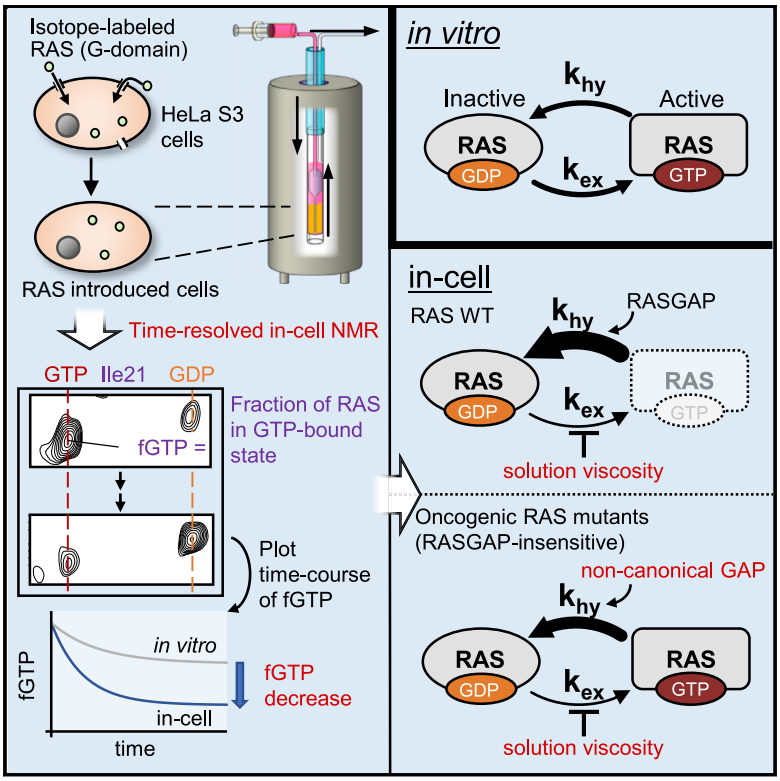

Highlights

- In-cell NMR reveals the time course of active GTP-bound RAS in live cells
- The GTP-bound levels of RAS in live cells is significantly lower than *in vitro*
- Highly viscous environment in cells reduces the nucleotide exchange rate of RAS
- GTP hydrolysis of RAS mutants is promoted by unidentified cellular proteins

Authors

Qingci Zhao, Ryu Fujimiya, Satoshi Kubo, Christopher B. Marshall, Mitsuhiko Ikura, Ichio Shimada, Noritaka Nishida

Correspondence

ichio.shimada@riken.jp (I.S.), nnishida@chiba-u.jp (N.N.)

In Brief

Zhao et al. report the real-time, in-cell NMR monitoring of activated GTP-bound RAS in live cells. They found that the intracellular GTP-bound levels of RAS and oncogenic mutants are significantly lower than *in vitro*, due to reduction of nucleotide exchange rates and increase of GTP hydrolysis rates, caused by intracellular factors.

Zhao et al., 2020, Cell Reports *32*, 108074
August 25, 2020 © 2020 The Author(s).
https://doi.org/10.1016/j.celrep.2020.108074

Cell Reports

CellPress
OPEN ACCESS

Report

Real-Time In-Cell NMR Reveals the Intracellular Modulation of GTP-Bound Levels of RAS

Qingci Zhao,[1] Ryu Fujimiya,[1] Satoshi Kubo,[1] Christopher B. Marshall,[2] Mitsuhiko Ikura,[2] Ichio Shimada,[1,3,*] and Noritaka Nishida[1,4,5,*]

[1]Graduate School of Pharmaceutical Sciences, University of Tokyo, 7-3-1 Hongo, Bunkyo-ku, Tokyo 113-0033, Japan
[2]Princess Margaret Cancer Centre, University Health Network and Department of Medical Biophysics, University of Toronto, Toronto, ON M5G 1L7, Canada
[3]RIKEN Center for Biosystems Dynamics Research, 1-7-22 Suehiro-cho, Tsurumi-ku, Yokohama, Kanagawa 230-0045, Japan
[4]Graduate School of Pharmaceutical Sciences, Chiba University, 1-8-1 Inohana, Chuo-ku, Chiba 260-8675, Japan
[5]Lead Contact
*Correspondence: ichio.shimada@riken.jp (I.S.), nnishida@chiba-u.jp (N.N.)
https://doi.org/10.1016/j.celrep.2020.108074

SUMMARY

The small guanosine triphosphatase (GTPase) RAS serves as a molecular switch in signal transduction, and its mutation and aberrant activation are implicated in tumorigenesis. Here, we perform real-time, in-cell nuclear magnetic resonance (NMR) analyses of non-farnesylated RAS to measure time courses of the fraction of the active GTP-bound form (fGTP) within cytosol of live mammalian cells. The observed intracellular fGTP is significantly lower than that measured *in vitro* for wild-type RAS as well as oncogenic mutants, due to both decrease of the guanosine diphosphate (GDP)-GTP exchange rate (k_{ex}) and increase of GTP hydrolysis rate (k_{hy}). *In vitro* reconstitution experiments show that highly viscous environments promote a reduction of k_{ex}, whereas the increase of k_{hy} is stimulated by unidentified cytosolic proteins. This study demonstrates the power of in-cell NMR to directly detect the GTP-bound levels of RAS in mammalian cells, thereby revealing that the k_{hy} and k_{ex} of RAS are modulated by various intracellular factors.

INTRODUCTION

RAS belongs to a subfamily of small guanosine triphosphatase (GTPase) proteins comprising three functionally similar isoforms (HRAS, KRAS, and NRAS; Wennerberg et al., 2005). RAS acts as a molecular switch in cell signaling that is activated in response to stimulation of receptor tyrosine kinases and in turn binds and activates effector proteins that regulate various cellular functions, including cell division, motility, and survival (Simanshu et al., 2017). The guanine-nucleotide binding state of RAS cycles between guanosine diphosphate (GDP)-bound and GTP-bound states (Figure 1A). The GDP-bound state of RAS is inactive, and exchange from GDP to GDP induces conformational changes in the switch I (amino acids [aas] 30–38) and switch II (aas 60–78) regions, enabling the interaction with downstream effector molecules, including RAF kinases, RalGDS, and phosphatidylinositol 3-kinase (PI3K) (Milburn et al., 1990; Pai et al., 1990). RAS is a proto-oncogenic protein and is frequently mutated in various types of cancer (Fernández-Medarde and Santos, 2011). Mutations of RAS, most frequently at three hotspot codons encoding G12, G13, or Q61, cause aberrant activation of RAS primarily by impairing hydrolysis of GTP (Lu et al., 2016; Prior et al., 2012). Mutant RAS is thus recognized as an important drug target for anti-cancer therapy, although development of direct inhibitors of RAS has been a challenge (Cox et al., 2014; Downward, 2003; McCormick, 2016; Papke and Der, 2017).

The intrinsic level of activation of RAS (i.e., the GTP loading) is determined by several parameters, including the relative concentrations of GDP and GTP present, the relative affinities of RAS for GDP and GTP, the GTP hydrolysis rate (k_{hy}), and the GDP-GTP exchange rate (k_{ex}). We previously reported a method to estimate k_{hy} and k_{ex} of RAS by observing the time-dependent changes in NMR signal intensities of cross-peaks specific to the GTP- and GDP-bound states in real time (Marshall et al., 2012; Smith et al., 2013). It was demonstrated that, compared to wild-type RAS (RAS WT), the oncogenic mutants G12V and Q61L exhibited 10- and 80-fold decreases in k_{hy}, respectively, although another mutation G13D causes a more modest 3-fold reduction in k_{hy} while increasing k_{ex} by 15-fold. Thus, the elevated state of activation of each oncogenic RAS mutant is caused by different contributions of decreased k_{hy} or increased k_{ex}.

The activation level of RAS is correlated to the fraction of RAS bound to GTP ($[RAS_{GTP}]/([RAS_{GTP}] + [RAS_{GDP}])$) hereafter referred to as fGTP. The fGTP in the steady state, which reflects the intrinsic activation level (i.e., in the absence of regulation by other proteins), can be determined by the following equation: $k_{ex}/(k_{hy} + k_{ex})$. Based on previously determined k_{hy} and k_{ex} values at 25°C (Smith et al., 2013), the fGTP of RAS WT is calculated to

This is an open access article under the CC BY-NC-ND license (http://creativecommons.org/licenses/by-nc-nd/4.0/).

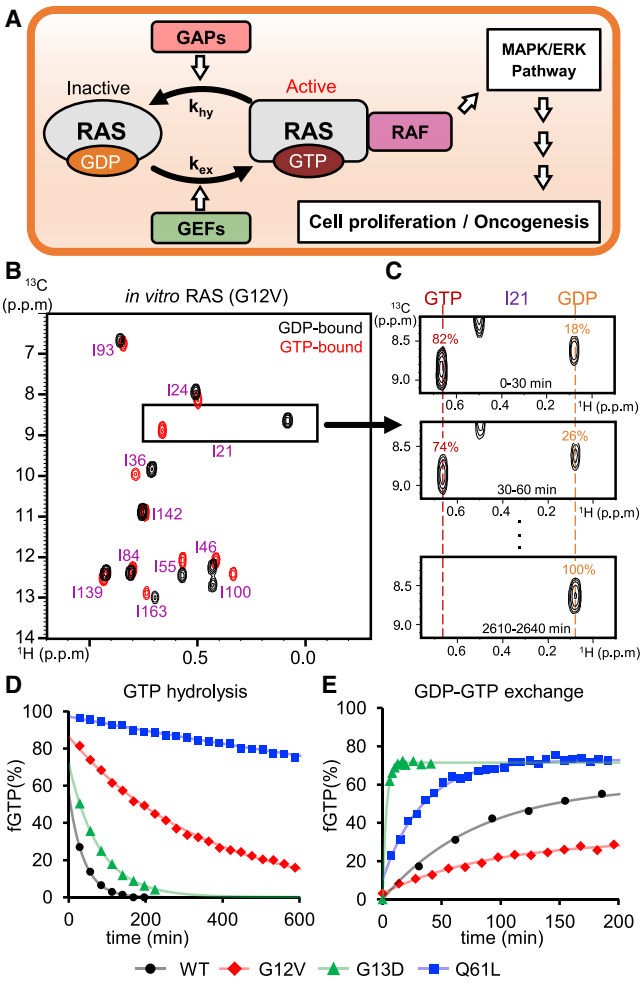

Figure 1. *In Vitro* NMR Measurements of k_{hy} and k_{ex} of RAS Using the Conventional Method

(A) GTPase cycle of RAS and signaling intracellular pathway. GTP-bounded RAS interacts effectors, such as RAF, causing activation of mitogen-activated protein kinase (MAPK)/extracellular signal-regulated kinase (ERK) signal pathway and cell proliferation. The GDP-GTP exchange is facilitated by GEFs. GTP hydrolysis is enhanced by the activity of GAPs.

(B) Overlaid 2D ^{1}H-^{13}C HSQC spectra of Ileδ1 methyl ^{13}C-labeled RAS G12V bound to GDP (black) or GTP (red). The spectrum of GTP-bound RAS was obtained from the first spectrum of following k_{hy} measurement immediately after GTP loading. The assignments of each peak are shown by purple.

(C) Time-dependent changes of I21 signals of GTP-loaded RAS G12V.

(D) Real-time monitoring of intrinsic GTP hydrolysis for RAS WT (black), G12V (red), G13D (green), and Q61L (blue) in 37°C. RAS proteins were loaded with GTP, and decays of the signal intensity ratio of I21 were monitored by sequential HSQCs.

(E) Real-time monitoring of GDP-GTP exchange reactions for RAS WT (black), G12V (red), G13D (green), and Q61L (blue) at 37°C. The exchange of GDP to GTPγS-bound RAS was observed in the presence of 2-fold molar excess GTPγS. k_{hy} and k_{ex} values of RAS WT and mutants were obtained from a single experiment by non-linear curve fitting.

For the entire plots of the GDP-GTP exchange reactions in the respective experiments, see Figures S1D–S1G. See also Table S1.

be ~30%, although the predicted fGTP of oncogenic mutants is elevated (69% for G12V, 95% for G13D, and 99% for Q61L), reflecting their constitutive activation. Based on the intrinsic k_{hy} and k_{ex} rates, approximately one-third of RAS WT would exist in an active GTP-bound state; however, cell-based studies show that RAS WT is largely inactive in the resting state and the biological role of RAS in signal transduction requires spatiotemporal regulation of its activation (Young et al., 2013).

Intracellular RAS proteins are regulated by a complex signaling network of endogenous proteins. GTP hydrolysis is accelerated by GTPase-activating proteins (GAPs), and GDP-GTP exchange is facilitated by guanine nucleotide exchange factor (GEF) proteins (Figure 1A; Bollag and McCormick, 1991; Boriack-Sjodin et al., 1998; Scheffzek et al., 1997). The effects of these intracellular regulatory molecules must be considered in order to predict the GTP-bound levels of RAS in a native cellular environment. The conventional biochemical approach to measure RAS activation in cells is a pull-down assay using immobilized RAS-binding domain (RBD) of an effector protein (e.g., c-RAF), which selectively captures GTP-bound RAS (Taylor et al., 2001). These assays provide a "snapshot" of the RAS activation but do not provide kinetic parameters of the GTPase cycle.

In this study, we utilized real-time, in-cell nuclear magnetic resonance (NMR) to monitor the GTPase cycle of RAS WT and three oncogenic mutants in a native cellular environment by introducing the RAS G-domain constructs lacking the C-terminal lipid-modification site into HeLa S3 cells. We evaluated the fGTP in the context of intracellular regulatory systems through time-resolved NMR measurements.

RESULTS

In Vitro Measurements of k_{hy} and k_{ex} of RAS Using the GTP Regeneration System Are Consistent with the Conventional Method

To obtain sufficient sensitivity to observe the NMR signals of RAS in live cells, we prepared selectively labeled RAS (HRAS GTPase domain [residues 1–171] without the C-terminal hypervariable region [HVR]; see STAR Methods for details) with ^{13}C Ileδ1 methyl group in ^{2}H background for methyl transverse relaxation optimized spectroscopy (TROSY) detection (Tugarinov et al., 2003). Before proceeding to introduce this protein into live cells, we performed extensive *in vitro* characterization. In both the GDP- and GTP-bound forms of RAS, we observed 11 signals corresponding to the 11 Ile residues in the protein. Half of these residues exhibit distinctive chemical shifts when bound to GDP versus native GTP or a GTP analog (Figure 1B), and we chose Ile21 to measure fGTP, because its pair of peaks were the best resolved due to the ring current effect from Tyr32 in switch I region in the GDP-bound state (Figure S1A). To calculate intrinsic GTP hydrolysis rates (k_{hy}), heteronuclear single-quantum correlation spectroscopy (HSQC) spectra of GTP-loaded RAS WT and mutants (200 μM; at 37°C) were acquired every 30 min (Figure 1C), and the time-dependent decays of fGTP were fit to an exponential decay curve (Figure 1D). The obtained k_{hy} value of RAS using Ile21 signal was almost identical with those obtained by using other Ile signals, such as Ile55 and Ile100 (Figures S1H–S1K). RAS WT and its mutants exhibited almost the same spectral pattern, except for the slight chemical shift difference in the signal of Ile21 in GDP-bound state (Figure S1B), presumably due to the local fluctuation of the Tyr32

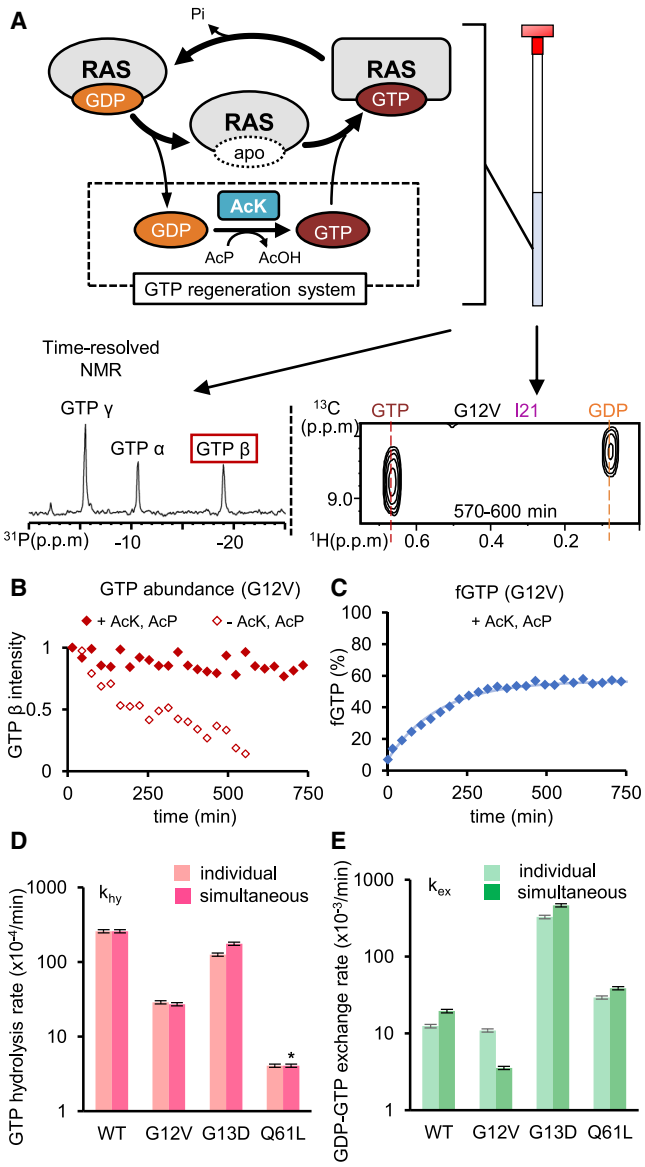

Figure 2. *In Vitro* Measurements of k_{hy} and k_{ex} of RAS Using the GTP Regeneration System

(A) Schematic illustration of the *in vitro* GTP regeneration system to measure the k_{hy} and k_{ex} of RAS simultaneously. GDP released from RAS was regenerated to GTP by acetate kinase (AcK), which transfers the phosphate group of acetyl phosphate (AcP) to GDP.

(B and C) The free GTP abundance (B) and time course of fGTP (C) of RAS G12V under the *in vitro* GTP regeneration system. The free GTP abundance without the system was represented by outlined diamond in (B). The time-dependent changes of free GTP abundance were estimated based on the signal intensity of β-phosphate of GTP as normalized by that of the first time point (for RAS WT and other mutants, see Figure S2).

(D) *In vitro* GTP hydrolysis rate (k_{hy}) of RAS WT and mutants measured in the GTP regeneration system (magenta) or by individual method (light magenta).

(E) *In vitro* GDP-GTP exchange rate (k_{ex}) of RAS WT and mutants measured in the GTP regeneration system (green) or by individual method (light green). All k_{hy} and k_{ex} values were obtained from a single experiment by non-linear curve fitting. Note that k_{hy} of RAS Q61L is too slow to directly measure in the GTP regeneration system. Therefore, the individually measured k_{hy} value (indicated as an asterisk) was used to calculate k_{ex} value.

Error bars in the bar graphs represent the uncertainty associated with rates derived from the fittings. See also Table S3.

side chain, as suggested by the crystal structure of the G13D mutant (Figure S1C). Compared to RAS WT, k_{hy} of the RAS oncogenic mutants G12V, G13D, and Q61L were reduced by 10-, 2-, and 80-fold, respectively (Table S1). We also measured successive HSQC spectra of GDP-loaded RAS WT and mutants (200 μM; at 37°C) in the presence of a 2-fold molar excess of GTPγS (a non-hydrolysable GTP analog) to measure the GDP-GTP exchange rate (k_{ex}) (Figure 1E). Compared to RAS WT, G12V showed slightly (13%) lower k_{ex}, although Q61L showed a 2.6-fold increase, and G13D exhibited a substantially faster exchange rate, 26-fold faster than RAS WT (Table S1). All these k_{hy} and k_{ex} values measured at 37°C are consistent with those measured in our previous study using ^{15}N amide signals at 25°C (Smith et al., 2013); each mutant induced similar changes in these rates relative to RAS WT (Table S2).

In the cell, GTP hydrolysis and GDP-GTP exchange reactions progress simultaneously in an environment where the native GTP concentration is maintained in excess to that of GDP (Traut, 1994). To reproduce this condition *in vitro* as a reference for subsequent in-cell NMR experiments, we established a "GTP-regeneration system" (Small and Addinall, 2003), in which GDP released from RAS following GTP hydrolysis was regenerated to GTP by acetate kinase (AcK), which transfers the phosphate group of acetyl phosphate (AcP) to GDP (Figure 2A). The advantage of this method is that the k_{hy} and k_{ex} can be obtained simultaneously under a condition where excess GTP is maintained (without competing with the released GDP), and these results can be used as *in vitro* reference for the subsequent in-cell NMR measurements. We measured the HSQC spectra of 200 μM GDP-loaded RAS G12V in the presence of 400 μM free GTP and simultaneously collected ^{31}P NMR spectra to confirm that the GTP/GDP ratio was maintained by the GTP-regeneration components (Figure 2A). In the absence of the GTP regeneration system, the ^{31}P signals of free GTP decayed rapidly as expected; however, these signals remained constant when GTP regeneration components were added, indicating that the concentration of GTP was successfully maintained in excess to GDP (Figure 2B). When RAS G12V, starting from the GDP-bound form, was introduced into this system, the fGTP reached the steady state with 57% bound to GTP after 300 min (Figure 2C). The GTP hydrolysis and GDP/GTP exchange rates can be deduced simultaneously by fitting the time course of the fGTP (see STAR Methods for details). The k_{hy} and k_{ex} values obtained by simultaneous fitting were almost identical to those obtained by the individually measured k_{hy} and k_{ex} rates for RAS WT and oncogenic mutants (Figures 2D, 2E, and S2A–S2F), except for the k_{ex} of G12V, which was lower (see the Discussion for detail). Additionally, we compared the k_{hy} and k_{ex} values determined for RAS WT and G12V mutant, when starting with the GTP- versus the GDP-bound form. The same k_{hy} and k_{ex} values, and steady-state fGTP, were obtained regardless of the starting fGTP (Figures S2G and S2H). These results indicate the initial GTP-loading state does not affect fGTP in the steady state and k_{hy} and k_{ex}.

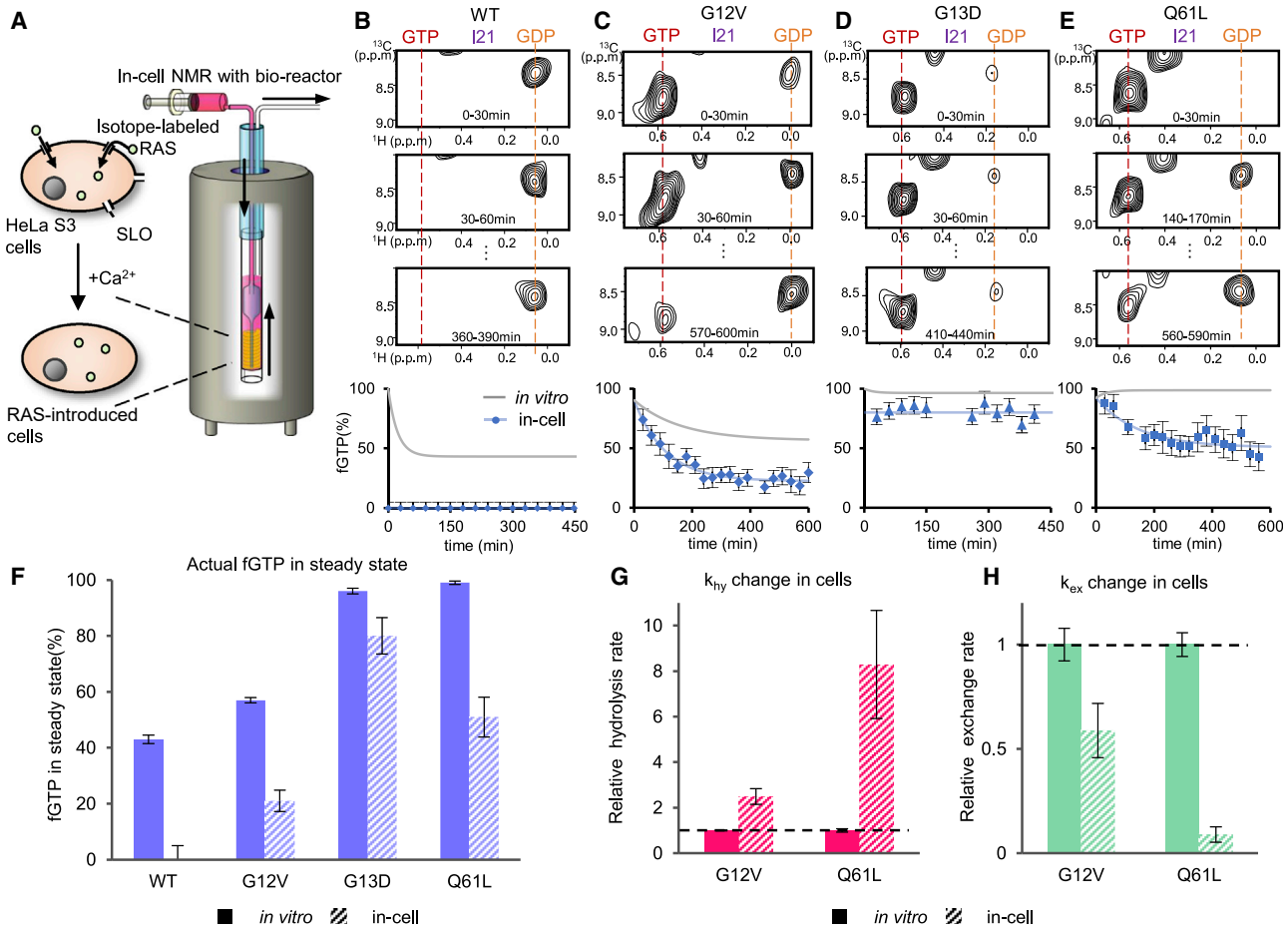

Figure 3. The Intracellular fGTP of RAS WT and the Oncogenic Mutants Is Lower Than *In Vitro* due to Increase of k_{hy} and Decrease of k_{ex}

(A) The schematic illustration of the method to observe the fraction of RAS bound to GTP in the cellular environments using in-cell NMR. Isotopically labeled RAS-GTP was introduced into HeLa S3 cells through a streptolysin O pore. Pores were sealed by addition of Ca^{2+}, and cells were immobilized in Mebiol gel in an NMR tube, which was perfused with medium.

(B–E) The time-resolved ^{1}H-^{13}C SOFAST HMQC spectra of GTP-loaded RAS WT (B), G12V (C), G13D (D), and Q61L (E) at representative time points. The position of I21 of GTP- and GDP-bound form is indicated by dotted line, and estimated fGTP at each time point was plotted at bottom with error bars calculated based on the signal-to-noise ratio of I21 (blue). For RAS WT (B) and G13D (D), the steady-state fGTP was estimated as an average of fGTP of all time points (indicated by blue line). For RAS G12V (C) and Q61L (E), the k_{hy}, k_{ex}, and the steady-state fGTP were estimated by curve fitting of experimental data (indicated by blue line; see text for detail). The gray lines indicate the theoretical time course of fGTP deduced from the *in vitro* k_{hy} and k_{ex} values. 3.0×10^7 cells were used for each in-cell NMR experiment.

(F) Summary of the steady-state fGTP of RAS WT and mutants measured *in vitro* (solid) and in cell (solid). Error bars of the bar graphs represent the uncertainty associated with rates derived from the fittings except for RAS WT and G13D in cell. The error bars of RAS WT and G13D in cell was estimated by based on the signal-to-noise ratio.

(G and H) The comparison of k_{hy} (G) and k_{ex} (H) of RAS G12V and Q61L *in vitro* (solid) and in cell (mesh). k_{hy} and k_{ex} values were normalized to those *in vitro* (indicated by dotted lines). All in-cell NMR data were generated from a single experiment.

Error bars in the bar graphs represent the uncertainty associated with rates derived from the fittings. See also Table S3.

The Intracellular fGTP of RAS WT and the Oncogenic Mutants Is Lower Than *In Vitro* due to Increase of k_{hy} and Decrease of k_{ex}

To observe the fraction of intracellular RAS bound to GTP in native cellular environments, we performed in-cell NMR measurements (Figure 3A). Ile δ1 methyl ^{13}C-labeled RAS was loaded with GTP and introduced into HeLa S3 cells along with the FITC (fluorescein isocyanate)-labeled RAS using the pore-forming toxin streptolysin O (SLO), and the pores were resealed by addition of Ca^{2+}-containing buffer (Ogino et al., 2009). The fluorescence microscopic imaging demonstrated that the exogenously introduced non-farnesylated RAS was distributed almost uniformly in the cytosol, as expected (Figure S3A). These cells were then immobilized within a thread of polymerized Mebiol gel formed inside an NMR tube, which was continuously perfused with a fresh culture medium during the NMR measurements (Kubo et al., 2013). In addition to feeding the cells, the perfusion system removes any protein that may leak from the cells. We analyzed the viability of these RAS-containing cells before and after NMR measurements using a flow cytometer,

confirming ~70% of cells were kept alive during measurements, regardless of RAS WT and oncogenic mutants (Figure S3B; Table S4). We acquired band-selective optimized flip angle short transient (SOFAST) ^{1}H-^{13}C heteronuclear multiple quantum correlation (HMQC) spectra (Schanda et al., 2005) of RAS-containing cells successively every 30 min. In the in-cell NMR spectrum of RAS G12V measured at the first time point, signals of all eleven Ile were observed, their chemical shift patterns were similar to those observed *in vitro*, and, with the exception of Ile139, there were no appreciable overlapping background signals derived from the natural abundance of ^{13}C in the medium or endogenous cellular proteins (Kubo et al., 2013; Figures S3C and S3D). Based on the signal intensities of the GTP- and GDP-bound states of RAS, it was estimated that 74% of RAS G12V was loaded with GTP for the first 30 min. The fGTP gradually decreased and reached the steady state at ~20% after 300 min (Figure 3C). We also performed similar in-cell NMR measurements for RAS WT (Figure 3B), G13D (Figure 3D), and Q61L (Figure 3E), which reached the steady state at <5%, ~80%, and ~50%, respectively. Compared to the *in vitro* experiments, RAS WT and all the mutants tested exhibited lower fGTPs in cells (Figure 3F). Notably, RAS WT exists predominantly in an inactive GDP-bound state, which is consistent with the previous cell biological estimation (Young et al., 2013). Although RAS Q61L showed higher fGTP than G13D in the *in vitro* measurements, G13D exhibited higher fGTP than Q61L in the in-cell NMR experiments, indicating that the fraction of active GTP-bound state of intracellular RAS mutants in the cellular environment cannot be predicted from their intrinsic hydrolysis and exchange properties *in vitro*.

The in-cell NMR observations of the GTP-bound fractions of RAS G12V and Q61L exhibited time-dependent decreases, enabling their intracellular k_{hy} and k_{ex} values to be estimated by curve fitting, as performed in the *in vitro* study (Figures 3C and 3E). RAS WT and G13D achieved steady state rapidly in the first spectrum collected precluding determination of these values. In comparison to the k_{hy} values obtained *in vitro*, RAS G12V and Q61L exhibited 2.5-fold and 8.3-fold faster rates in cells, respectively (Figure 3G). On the other hand, in cells, nucleotide exchange was slower; k_{ex} of RAS G12V and Q61L were reduced by 41% and 91%, respectively (Figure 3H). These results indicate that both increased hydrolysis and decreased exchange rates contribute to decreased fGTP of RAS in the cell.

The Reduction of Intracellular k_{ex} Is Caused by Highly Viscous Environments

In-cell NMR experiments revealed the intrinsic hydrolysis and exchange rates (k_{hy} and k_{ex}) of RAS WT and oncogenic mutants were modulated under the intracellular environments. GAP proteins likely contributed to the intracellular k_{hy} increase observed for RAS WT (Figure 1A). However, the RAS mutants, which are known to exhibit severely reduced sensitivity to the activity of RASGAP (Gideon et al., 1992; Hunter et al., 2015; Smith et al., 2013), also exhibited increased GTP hydrolysis in cells. Guanine nucleotide dissociation inhibitors (GDIs) are cellular proteins that decrease GDP-GTP exchange of particular small GTPases of the RHO and RAB subfamilies; however, the observed reductions in k_{ex} are probably not caused by GDIs because none are known for RAS (Cherfils and Zeghouf, 2013). Therefore, we explored other cellular factors that modulate the k_{hy} and k_{ex} of RAS.

The intracellular environment experiences macromolecular crowding (MC), whereby proteins and metabolites are densely packed at very high concentrations. It is known that MC can modulate protein function by non-specific interactions and size-exclusion effects and reduced diffusion rates caused by high solution viscosity (Ellis, 2001). To investigate whether the intracellular MC environment influences k_{hy} and k_{ex} of RAS, we mimicked crowding effects using molecular crowding reagents, such as bovine serum albumin (BSA) for non-specific interactions, the polysaccharide Ficoll for volume exclusion effects, and glycerol to increase solution viscosity (Figures 4A, 4B, and S4A–S4F). The concentrations of the crowding agents were adopted from the previous NMR studies, which investigated the MC effects (Wang et al., 2010; Theillet et al., 2016). We did not observe any significant increase for k_{hy} or decrease of k_{ex} for RAS WT in the presence of 300 mg/mL BSA or 200 mg/mL Ficoll. Rather, the addition of BSA slightly increased k_{ex}, suggesting that the observed cellular effects on RAS WT are not likely to be attributed to non-specific interactions or volume exclusion effects. Interestingly, the k_{hy} of RAS WT increased by 57% in the presence of 30% (w/v) glycerol; however, the addition of glycerol did not alter the k_{hy} of the oncogenic RAS mutants (Figures 4C and S4G–S4I). This suggests that the increase of k_{hy} (for the mutants) in the cells is not related to the high viscosity of the intracellular environment. On the other hand, the presence of glycerol decreased the k_{ex} values of RAS WT as well as the oncogenic mutants by 30%–50%, indicating that the high viscosity of the intracellular environment may contribute to the decreased k_{ex} (Figures 4D and S4J–S4L). Although Ile signals exhibited the line broadening due to the increased rotational correlation time in the highly viscous environments, no appreciable chemical shift changes were observed in the NMR spectrum of RAS upon addition of glycerol (Figures S4M–S4O), suggesting the decreased k_{ex} is not due to conformational changes. We speculate that reduced diffusion in the viscous solution may promote rebinding of GDP after it is released from RAS, thus competing with the productive nucleotide exchange with GTP and decreasing the apparent k_{ex} (Figure 4E).

Increase of Intracellular k_{hy} Is Caused by Cytosolic Proteins

Because MC did not increase the k_{hy} for the RAS mutants, we investigated whether specific endogenous cellular components enhance the GTPase activity of RAS. We measured the k_{hy} of G12V in the presence of the cell lysate derived from HeLa S3 cells and compared to the k_{hy} measured in the absence of lysate (Figures 4F and S5A–S5C). Indeed, the k_{hy} was increased by 2.2-fold in the presence of the lysate, and this effect was retained after removal of the insoluble fraction; however, it was abolished by heat denaturation (Figure 4G), suggesting that the lysate contains a specific soluble cytoplasmic heat-sensitive macromolecule that can facilitate hydrolysis of GTP by this oncogenic RAS mutant. We examined the molecular size of this cellular component by fractionating the cell lysate by ultra-filtration (Figures 4H and S5D–S5G). The factor that promoted RAS GTPase activity passed through 50- and 100-kDa molecular

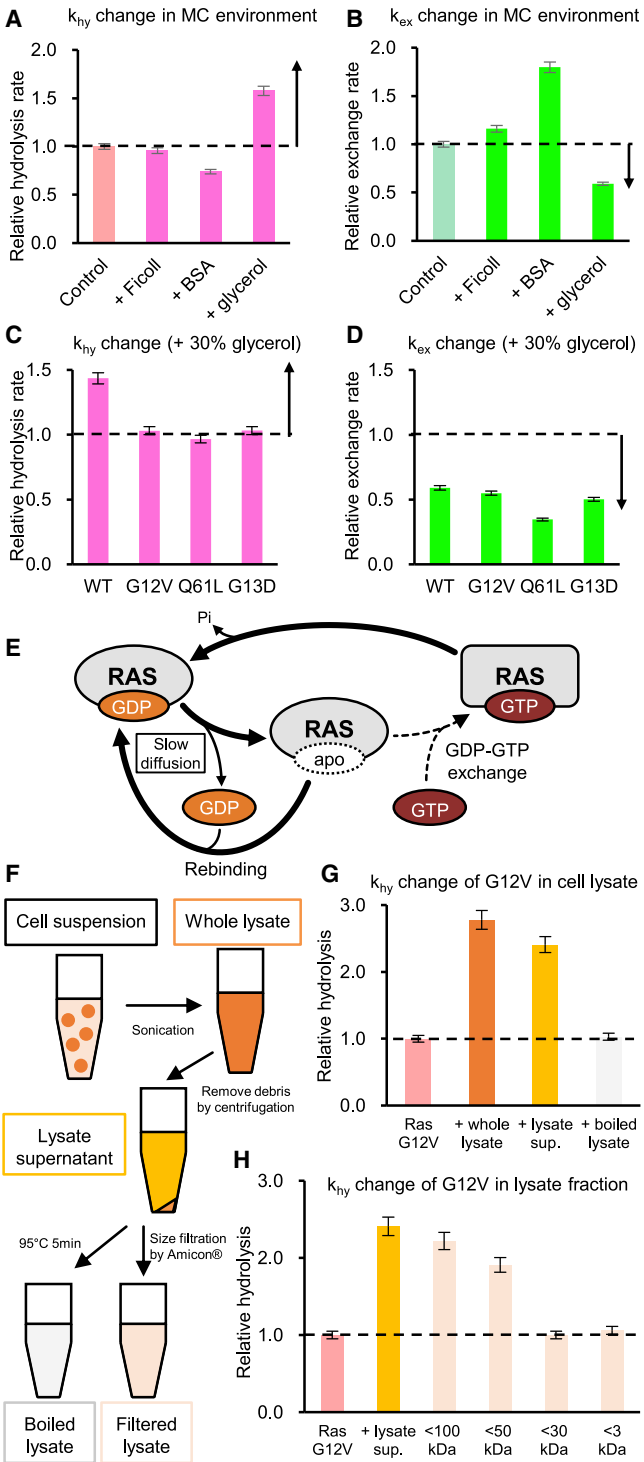

Figure 4. The Reduction of Intracellular k_{ex} Is Caused by Highly Viscous Environments, and the Increase of k_{hy} of RAS Is Stimulated by Cytosolic Proteins

(A and B) k_{hy} (A) and k_{ex} (B) of RAS WT measured in the presence of crowder reagents (200 mg/mL Ficoll, 200 mg/mL BSA, and 30% [w/v] glycerol). k_{hy} and k_{ex} values were normalized to those without crowder reagents (indicated by dotted line). See also Table S5.

(C and D) k_{hy} (C) and k_{ex} (D) of RAS WT and mutants measured in the presence of 30% (w/v) glycerol. k_{hy} and k_{ex} values were normalized to those without glycerol (indicated by dotted lines). The arrows on the graphs indicate the increase for k_{hy} and decrease of k_{ex}, which are related to those changes in the cellular environments. The error bars on the graphs correspond to the standard deviations from the fittings. See also Table S6.

(E) A schematic model for the decrease of GDP-GTP exchange rate. In a highly viscous environment, the rebinding of released GDP occurs preferentially over the GTP binding, possibly due to slow diffusion rate, resulting in the decrease of apparent k_{ex} of RAS.

(F) Schematic of preparation and fractionation of cell lysates by size.

(G) GTP hydrolysis rates of RAS G12V in the presence of the whole lysate, lysate supernatant (referred to as lysate sup.), and boiled lysate. All k_{hy} values were normalized by those measured without cell lysate (indicated by dotted lines).

(H) GTP hydrolysis rate of RAS G12V in the presence of MW size-fractionated lysates (MW < 100 kDa, <50 kDa, <30 kDa, and <3 kDa). k_{hy} and k_{ex} values were obtained from a single experiment by non-linear curve fitting.

Error bars in the bar graphs represent the uncertainty associated with rates derived from the fittings. See also Table S7.

weight cut-off (MWCO) membranes but did pass through a 30-kDa MWCO membrane (Figure 4H), indicating that its apparent molecular weight (MW) falls between 30 and 50 kDa. Retention of this factor by a 30-kDa MWCO membrane rules out the possibility that the observed conversion of RAS-GTP to RAS-GDP could have been the result of "back exchange" with cell-derived GDP in the lysate. The observed activity is unlikely to be a known RASGAP for several reasons: (1) although the G12V mutant has not been tested for sensitivity to all known RASGAPs, their sequence and active site conservation suggest they all work through the same catalytic mechanism, which is impaired by the mutation (Scheffzek and Shivalingaiah, 2019; Scheffzek et al., 1997). (2) All known RASGAPs are larger than 50 kDa (Scheffzek and Shivalingaiah, 2019), and although proteolytic fragments or potential (unknown) smaller splice variants might be capable of passing through the 50-kDa membrane, there was no activity retained by the 100-kDa membrane, where most RASGAP activity would be expected to be found. This result is consistent with the presence of a heat-sensitive macromolecule that is capable of promoting GTP hydrolysis by the catalytically impaired RAS G12V mutant, likely through a mechanism that differs from the catalytic arginine finger in RASGAPs.

DISCUSSION

In this study, we performed in-cell NMR experiments to measure the fraction of RAS in the GTP-bound state (fGTP) under the intracellular condition. The fGTP is the measure of the extent of activation of RAS and thus critically important to quantify the fGTP in the intracellular context, which is related to onset of RAS-related diseases. As performed in the current study, the *in vitro* fGTP at steady state either indirectly deduced based on individual k_{hy} and k_{ex} measurements or directly measured in the GTP regeneration system indicated that ~40% of RAS WT is in an active GTP-bound state. On the contrary, in-cell NMR measurements of fGTP demonstrated that RAS WT is maintained predominantly in an inactive GDP-bound state. In addition, other RAS oncogenic mutants exhibited constitutive activation *in vitro*, but their fGTP is significantly reduced in the

cell. Therefore, RAS can be intrinsically highly activated; however, the effective downregulation by signaling components (such as GAP) and the intracellular environment (such as membrane-associated subcellular location and MC) enables RAS to function as a molecular switch.

In this study, we measured *in vitro* k_{hy} and k_{ex} using two methods, the individual and the simultaneous methods. Although almost the same values were obtained *in vitro*, the k_{ex} of G12V was different between the two methods. In the individual nucleotide exchange assay for measuring k_{ex}, where 2-fold excess free GTPγS was added to GDP-loaded RAS, the steady-state fGTP would become theoretically 67% if RAS has no binding preference for GTP and GDP. Consistent with this assumption, the steady-state fGTP was 60%–70% for RAS WT, G13D, and Q61L (Figures 1E, S1D, S1F, and S1G); however, RAS G12V showed significantly lower plateau value of fGTP (Figures 1E and S1E), possibly because G12V has higher affinity for GDP than GTP (analog), resulting in inaccurate k_{ex} estimation. In contrast, in the GTP regeneration system, the k_{ex} values would not be affected by the relative affinities for GTP and GDP, because GDP concentration is maintained much lower than GTP. Therefore, the GTP regeneration system provides a more accurate estimate of k_{ex} values, even for mutants that alter GDP/GTP binding preferences. When we estimated the intracellular k_{hy} and k_{ex} by in-cell NMR using the simultaneous method, the concentration of GTP is assumed to be excess to GDP (Traut, 1994). Although we have not directly measured the intracellular GTP/GDP concentration in HeLa S3 cells during the experiments, the in-cell NMR observation of RAS G13D, which has no binding preference for GTP and GDP, showed more than 80% fGTP, indicating that GTP is maintained in excess over GDP in these cells.

As a first step for in-cell NMR studies of RAS, we chose to use a RAS construct lacking the C-terminal HVR, mainly due to technical reasons, such as low NMR sensitivity for membrane-bound farnesylated RAS. Native RAS contains a "CAAX" motif at the C terminus of the HVR, which is subjected to multiple post-translational modifications (Ahearn et al., 2011; Wright and Philips, 2006), including prenylation of the cysteine residues (Del Villar et al., 1996), removal of the AAX tripeptide (Bergo et al., 2008; Boyartchuk et al., 1997), and methylation of the C-terminal cysteine (Dai et al., 1998). These modifications promote the localization of RAS to the plasma membrane, which is important for signal transduction mediated by membrane-localized upstream regulatory molecules, especially GEFs, but also some GAPs (Scheffzek and Shivalingaiah, 2019). In this study, we found that RAS WT exists predominantly in an inactive GDP-bound state, although other oncogenic mutants exhibited distinct populations of the active GTP-bound state. This observation suggests that the fGTP of RAS lacking the HVR, which predominantly resides in the cytoplasm, could reflect the basal activation level of RAS in the resting cell (in which ligand-induced upstream signaling is seized). We propose that the detection of the fGTP in live cells is important, as this enables us to monitor the real level of activated, oncogenic RAS mutants, which have been believed to be "hyper-activated," regardless of the upstream signaling. Hence, this tool may be used as a "readout" to assess the efficacy of potential inhibitors for RAS within the intracellular context. In future experiments, signaling-dependent RAS activation could be observed by introducing isotopically labeled farnesylated and fully processed RAS, which can be produced in an insect cell/baculovirus expression system (Gillette et al., 2015). Alternately, endogenous farnesyl transferase (FTase) and RAS processing enzymes may be sufficient to modify exogenous full-length RAS after it is introduced into cells; however, this remains to be investigated. We previously demonstrated that it is possible to observe NMR signal of KRAS tethered to lipid bilayers in nanodisc (Mazhab-Jafari et al., 2015; Fang et al., 2018; Lee et al., 2020). The nanodisc experiments indicated that the GTPase domain of KRAS remains somewhat mobile and tumbles semi-independently of the nanodisc, even though the farnesylated HVR is more tightly associated with the plasma membrane. In addition, those previous researches using nanodiscs suggested that the membrane-tethered KRAS adopts multiple orientations with respect to membrane (Mazhab-Jafari et al., 2015), and RAS dimerizes on membrane surface at α4-5 helix (Lee et al., 2020). Therefore, in-cell NMR experiments using the intact farnesylated RAS will clarify how the interactions on plasma membrane affect the k_{hy} or k_{ex} of RAS.

We found that the decrease of fGTP in the intracellular condition results from both an increase of k_{hy} and a decrease of k_{ex}. Using a variety of MC reagents, we found that higher viscosity in the presence of 30% glycerol causes decrease of k_{ex} for the RAS WT as well as oncogenic mutants. A number of studies have demonstrated that various protein activities are affected in high-viscosity solutions. For example, the catalytic rate of carbonic anhydrase, which diffusion limited (Lindskog, 1997), becomes slower in glycerol and sucrose solutions, but not in Ficoll (Pocker and Janjić, 1987). Thus, we hypothesized such slower molecular diffusion in highly viscous cytosolic environments may decrease k_{ex} by competing the exchange of GDP to GTP with rebinding of released GDP. We also observed an increase of k_{hy} in the presence of glycerol; however, this was observed only for RAS WT. A crystal structure of HRAS in complex with GTP analog (Pai et al., 1990) showed that the catalytic water molecule is coordinated near the γ-phosphate of GTP. We speculate that stabilization of this catalytic water by glycerol facilitates the GTP hydrolysis of RAS WT but has less impact on the oncogenic mutants because their GTPase activities are intrinsically low. We found that the GTPase activity was enhanced by addition of cell lysate. Although this result was expected for RAS WT, it was rather surprising to observe this for the oncogenic mutant G12V, which is known to be insensitive to RASGAP (Gideon et al., 1992). In addition, size fractionation of the cell lysate indicates the molecule(s) responsible for increasing k_{hy} fractionated with the MW range 30–50 kDa, which is much smaller than the known canonical RASGAPs in the intracellular environment (Scheffzek and Shivalingaiah, 2019). This result is consistent with the presence of a heat-sensitive macromolecule that is capable of promoting GTP hydrolysis by the catalytically impaired RAS G12V mutant, likely through a mechanism that differs from the catalytic arginine finger in RASGAPs (Scheffzek et al., 1997). We are now undertaking a proteomics approach to identify these molecules that can promote RAS GTP hydrolysis. Identification of such regulatory molecules will help us to more deeply understand the regulation mechanisms of RAS in

physiological and pathological contexts and guide the development of drugs that inhibit the activation of RAS with alternative mechanisms of action.

In summary, we established the in-cell NMR method to measure the GTP-bound levels of RAS under native intracellular environments in a real-time manner, thereby revealing the intracellular fGTP was significantly lower than *in vitro* for WT as well as oncogenic mutants. This method demonstrates the power of in-cell NMR to directly evaluate the status of intracellular proteins under the influence of MC and endogenous regulatory molecules, which cannot be reconstituted *in vitro*. This method may provide a powerful tool to assess the efficacy in the intracellular context of drugs for target proteins, such as RAS, or their upstream regulatory proteins (e.g., inhibitors of Son of Sevenless (SOS) protein).

STAR★METHODS

Detailed methods are provided in the online version of this paper and include the following:

- KEY RESOURCES TABLE
- RESOURCE AVAILABILITY
  - Lead Contact
  - Materials Availability
  - Data and Code Availability
- EXPERIMENTAL MODEL AND SUBJECT DETAILS
- METHOD DETAILS
  - Protein Expression and Preparation
  - *In Vitro* NMR Experiments
  - Preparation of Cells for In-Cell NMR Measurements
  - In-Cell NMR Measurement Using the Bioreactor System
  - Preparation of Cell Lysates
- QUANTIFICATION AND STATISTICAL ANALYSIS

SUPPLEMENTAL INFORMATION

Supplemental Information can be found online at https://doi.org/10.1016/j.celrep.2020.108074.

ACKNOWLEDGMENTS

This work was supported in part by grants from the Japan Agency for Medical Research and Development (AMED) grant number JP18ae010104 (to I.S.); Japan Society for the Promotion of Science (JSPS) KAKENHI grant numbers JP17H06097 (to I.S.) and 26119005 and 20H04693 (to N.N.); the Naito Foundation (to N.N.); as well as the support from Canadian Institutes of Health Research (410008598), Canadian Cancer Society Research Institute (703209 and 706696), and Princess Margaret Cancer Foundation (to M.I.). M.I. is a Canada Research Chair in Cancer Structural Biology.

AUTHOR CONTRIBUTIONS

Q.Z., R.F., C.B.M., M.I., I.S., and N.N. designed the study; Q.Z., R.F., S.K., and N.N. purified proteins, constructed the mutants, performed *in vitro* and in-cell NMR experiments, and analyzed data with advice from C.B.M., M.I., and I.S.; and Q.Z., C.B.M., M.I., I.S., and N.N. wrote the manuscript.

DECLARATION OF INTERESTS

The authors declare no competing interests.

Received: April 23, 2020
Revised: July 3, 2020
Accepted: August 5, 2020
Published: August 25, 2020

REFERENCES

Ahearn, I.M., Haigis, K., Bar-Sagi, D., and Philips, M.R. (2011). Regulating the regulator: post-translational modification of RAS. Nat. Rev. Mol. Cell Biol. *13*, 39–51.

Bergo, M.O., Wahlstrom, A.M., Fong, L.G., and Young, S.G. (2008). Genetic analyses of the role of RCE1 in RAS membrane association and transformation. Methods Enzymol. *438*, 367–389.

Bollag, G., and McCormick, F. (1991). Differential regulation of rasGAP and neurofibromatosis gene product activities. Nature *351*, 576–579.

Boriack-Sjodin, P.A., Margarit, S.M., Bar-Sagi, D., and Kuriyan, J. (1998). The structural basis of the activation of Ras by Sos. Nature *394*, 337–343.

Boyartchuk, V.L., Ashby, M.N., and Rine, J. (1997). Modulation of Ras and a-factor function by carboxyl-terminal proteolysis. Science *275*, 1796–1800.

Cherfils, J., and Zeghouf, M. (2013). Regulation of small GTPases by GEFs, GAPs, and GDIs. Physiol. Rev. *93*, 269–309.

Cox, A.D., Fesik, S.W., Kimmelman, A.C., Luo, J., and Der, C.J. (2014). Drugging the undruggable RAS: Mission possible? Nat. Rev. Drug Discov. *13*, 828–851.

Dai, Q., Choy, E., Chiu, V., Romano, J., Slivka, S.R., Steitz, S.A., Michaelis, S., and Philips, M.R. (1998). Mammalian prenylcysteine carboxyl methyltransferase is in the endoplasmic reticulum. J. Biol. Chem. *273*, 15030–15034.

Del Villar, K., Dorin, D., Sattler, I., Urano, J., Poullet, P., Robinson, N., Mitsuzawa, H., and Tamanoi, F. (1996). C-terminal motifs found in Ras-superfamily G-proteins: CAAX and C-seven motifs. Biochem. Soc. Trans. *24*, 709–713.

Downward, J. (2003). Targeting RAS signalling pathways in cancer therapy. Nat. Rev. Cancer *3*, 11–22.

Ellis, R.J. (2001). Macromolecular crowding: obvious but underappreciated. Trends Biochem. Sci. *26*, 597–604.

Fang, Z., Marshall, C.B., Nishikawa, T., Gossert, A.D., Jansen, J.M., Jahnke, W., and Ikura, M. (2018). Inhibition of K-RAS4B by a unique mechanism of action: stabilizing membrane-dependent occlusion of the effector-binding site. Cell Chem. Biol. *25*, 1327–1336.e4.

Fernández-Medarde, A., and Santos, E. (2011). Ras in cancer and developmental diseases. Genes Cancer *2*, 344–358.

Gideon, P., John, J., Frech, M., Lautwein, A., Clark, R., Scheffler, J.E., and Wittinghofer, A. (1992). Mutational and kinetic analyses of the GTPase-activating protein (GAP)-p21 interaction: the C-terminal domain of GAP is not sufficient for full activity. Mol. Cell. Biol. *12*, 2050–2056.

Gillette, W.K., Esposito, D., Abreu Blanco, M., Alexander, P., Bindu, L., Bittner, C., Chertov, O., Frank, P.H., Grose, C., Jones, J.E., et al. (2015). Farnesylated and methylated KRAS4b: high yield production of protein suitable for biophysical studies of prenylated protein-lipid interactions. Sci. Rep. *5*, 15916.

Hunter, J.C., Manandhar, A., Carrasco, M.A., Gurbani, D., Gondi, S., and Westover, K.D. (2015). Biochemical and structural analysis of common cancer-associated KRAS mutations. Mol. Cancer Res. *13*, 1325–1335.

Kubo, S., Nishida, N., Udagawa, Y., Takarada, O., Ogino, S., and Shimada, I. (2013). A gel-encapsulated bioreactor system for NMR studies of protein-protein interactions in living mammalian cells. Angew. Chem. Int. Ed. Engl. *52*, 1208–1211.

Lee, K.-Y., Fang, Z., Enomoto, M., Gasmi-Seabrook, G., Zheng, L., Koide, S., Ikura, M., and Marshall, C.B. (2020). Two distinct structures of membrane-associated homodimers of GTP- and GDP-bound KRAS4B revealed by paramagnetic relaxation enhancement. Angew. Chem. Int. Ed. Engl. *59*, 11037–11045.

Lindskog, S. (1997). Structure and mechanism of carbonic anhydrase. Pharmacol. Ther. *74*, 1–20.

Lu, S., Jang, H., Nussinov, R., and Zhang, J. (2016). The structural basis of oncogenic mutations G12, G13 and Q61 in small GTPase K-Ras4B. Sci. Rep. *6*, 21949.

Marshall, C.B., Meiri, D., Smith, M.J., Mazhab-Jafari, M.T., Gasmi-Seabrook, G.M.C., Rottapel, R., Stambolic, V., and Ikura, M. (2012). Probing the GTPase cycle with real-time NMR: GAP and GEF activities in cell extracts. Methods *57*, 473–485.

Mazhab-Jafari, M.T., Marshall, C.B., Smith, M.J., Gasmi-Seabrook, G.M.C., Stathopulos, P.B., Inagaki, F., Kay, L.E., Neel, B.G., and Ikura, M. (2015). Oncogenic and RASopathy-associated K-RAS mutations relieve membrane-dependent occlusion of the effector-binding site. Proc. Natl. Acad. Sci. USA *112*, 6625–6630.

McCormick, F. (2016). K-Ras protein as a drug target. J. Mol. Med. (Berl.) *94*, 253–258.

Milburn, M.V., Tong, L., deVos, A.M., Brünger, A., Yamaizumi, Z., Nishimura, S., and Kim, S.H. (1990). Molecular switch for signal transduction: structural differences between active and inactive forms of protooncogenic ras proteins. Science *247*, 939–945.

Ogino, S., Kubo, S., Umemoto, R., Huang, S., Nishida, N., and Shimada, I. (2009). Observation of NMR signals from proteins introduced into living mammalian cells by reversible membrane permeabilization using a pore-forming toxin, streptolysin O. J. Am. Chem. Soc. *131*, 10834–10835.

Pai, E.F., Krengel, U., Petsko, G.A., Goody, R.S., Kabsch, W., and Wittinghofer, A. (1990). Refined crystal structure of the triphosphate conformation of H-ras p21 at 1.35 A resolution: implications for the mechanism of GTP hydrolysis. EMBO J. *9*, 2351–2359.

Papke, B., and Der, C.J. (2017). Drugging RAS: know the enemy. Science *355*, 1158–1163.

Pocker, Y., and Janjić, N. (1987). Enzyme kinetics in solvents of increased viscosity. Dynamic aspects of carbonic anhydrase catalysis. Biochemistry *26*, 2597–2606.

Prior, I.A., Lewis, P.D., and Mattos, C. (2012). A comprehensive survey of Ras mutations in cancer. Cancer Res. *72*, 2457–2467.

Schanda, P., Kupče, E., and Brutscher, B. (2005). SOFAST-HMQC experiments for recording two-dimensional heteronuclear correlation spectra of proteins within a few seconds. J. Biomol. NMR *33*, 199–211.

Scheffzek, K., and Shivalingaiah, G. (2019). Ras-specific GTPase-activating proteins-structures, mechanisms, and interactions. Cold Spring Harb. Perspect. Med. *9*, a031500.

Scheffzek, K., Ahmadian, M.R., Kabsch, W., Wiesmüller, L., Lautwein, A., Schmitz, F., and Wittinghofer, A. (1997). The Ras-RasGAP complex: structural basis for GTPase activation and its loss in oncogenic Ras mutants. Science *277*, 333–338.

Simanshu, D.K., Nissley, D.V., and McCormick, F. (2017). RAS proteins and their regulators in human disease. Cell *170*, 17–33.

Small, E., and Addinall, S.G. (2003). Dynamic FtsZ polymerization is sensitive to the GTP to GDP ratio and can be maintained at steady state using a GTP-regeneration system. Microbiology *149*, 2235–2242.

Smith, M.J., Neel, B.G., and Ikura, M. (2013). NMR-based functional profiling of RASopathies and oncogenic RAS mutations. Proc. Natl. Acad. Sci. USA *110*, 4574–4579.

Taylor, S.J., Resnick, R.J., and Shalloway, D. (2001). Nonradioactive determination of Ras-GTP levels using activated ras interaction assay. Methods Enzymol. *333*, 333–342.

Theillet, F.-X., Binolfi, A., Bekei, B., Martorana, A., Rose, H.M., Stuiver, M., Verzini, S., Lorenz, D., van Rossum, M., Goldfarb, D., and Selenko, P. (2016). Structural disorder of monomeric α-synuclein persists in mammalian cells. Nature *530*, 45–50.

Traut, T.W. (1994). Physiological concentrations of purines and pyrimidines. Mol. Cell. Biochem. *140*, 1–22.

Tugarinov, V., Hwang, P.M., Ollerenshaw, J.E., and Kay, L.E. (2003). Cross-correlated relaxation enhanced 1H-13C NMR spectroscopy of methyl groups in very high molecular weight proteins and protein complexes. J. Am. Chem. Soc. *125*, 10420–10428.

Wang, Y., Li, C., and Pielak, G.J. (2010). Effects of proteins on protein diffusion. J. Am. Chem. Soc. *132*, 9392–9397.

Wennerberg, K., Rossman, K.L., and Der, C.J. (2005). The Ras superfamily at a glance. J. Cell Sci. *118*, 843–846.

Wright, L.P., and Philips, M.R. (2006). Thematic review series: lipid posttranslational modifications. CAAX modification and membrane targeting of Ras. J. Lipid Res. *47*, 883–891.

Young, A., Lou, D., and McCormick, F. (2013). Oncogenic and wild-type Ras play divergent roles in the regulation of mitogen-activated protein kinase signaling. Cancer Discov. *3*, 112–123.

STAR★METHODS

KEY RESOURCES TABLE

REAGENT or RESOURCE	SOURCE	IDENTIFIER
Bacterial and Virus Strains		
Escherichia coli BL21(DE3) codon RP plus	Agilent	230250
Chemicals, Peptides, and Recombinant Proteins		
[^{15}N] Ammonium Chloride	Cambridge Isotope Laboratories	Cat#NLM-478-PK
[Methyl-^{13}C, 2,2-D_2] Alpha-ketobutyric Acid	Cambridge Isotope Laboratories	Cat#CDLM-7318-PK
[^{2}H] D-Glucose	ISOTEC	Cat#552003
D_2O	ISOTEC	Cat#617385
GTP	Sigma-Aldrich	Cat#G8877
GDP	Sigma-Aldrich	Cat#G7127
GTPγS	Sigma-Aldrich	Cat#G8634
Acetate Kinase	Sigma-Aldrich	Cat#A7437
Acetyl Phosphate	Sigma-Aldrich	Cat#A0262
Streptolysin O	Bio Academia	Cat#01-531
Mebiol Gel	Mebiol	Cat#PMW20
Albumin, from Bovine Serum (BSA), Fatty Acid Free	Wako	Cat#013-15143
Ficoll PM70	GE healthcare	Cat#17-0310-10
Experimental Models: Cell Lines		
Human: HeLaS3	JCRB	JCRB9010
Recombinant DNA		
Plasmid: pET-15b_HRAS(1-171)_WT	Smith et al., 2013	N/A
Plasmid: pET-15b_HRAS(1-171)_G12V	Smith et al., 2013	N/A
Plasmid: pET-15b_HRAS(1-171)_G13D	Smith et al., 2013	N/A
Plasmid: pET-15b_HRAS(1-171)_Q61L	Smith et al., 2013	N/A
Software and Algorithms		
TOPSPIN 3	Bruker/ Biospin	N/A
GraphPad Prism 8	Graphpad Software	https://www.graphpad.com/scientific-software/prism/
Other		
HIS-Select Nickel Affinity Gel	Sigma-Aldrich	Cat#P6611
HiLoad 26/600 Superdex 75 pg	GE Healthcare	Cat#28989334
CytoFlex Flow Cytometer	Beckman Coulter	Cat#B53000
Amicon Ultra-4 3kDa	Merck Millipore	Cat#UFC8003
Amicon Ultra-4 30kDa	Merck Millipore	Cat#UFC8030
Amicon Ultra-4 50kDa	Merck Millipore	Cat#UFC8050
Amicon Ultra-4 100kDa	Merck Millipore	Cat#UFC8100

RESOURCE AVAILABILITY

Lead Contact

Further information and requests for resources and reagents should be directed to and will be fulfilled by the Lead Contact, Noritaka Nishida (nnishida@chiba-u.jp).

Materials Availability

Plasmids generated in this study are available upon request from the Lead Contact.

Data and Code Availability

This study did not generate any unique datasets or code.

EXPERIMENTAL MODEL AND SUBJECT DETAILS

HeLa S3 cells obtained from JCRB (JCRB9010, Japan) were cultured in Dulbecco's modified eagle's medium (DMEM: GIBCO, Invitrogen, USA) containing 10% (v/v) fetal calf serum (FCS), L- glutamine, penicillin and streptomycin at 37°C with an atmosphere containing 5% CO_2.

METHOD DETAILS

Protein Expression and Preparation

The cDNA encoding HRAS GTPase domain (residues 1-171) was cloned into the pET-15b vector (NdeI-BamHI) which contains the 6x N-terminal His-tag and thrombin sequence. The plasmid was transformed into *Escherichia coli* (*E. coli*) BL21 (DE3) codon RP plus cells (Agilent technologies) and protein expression was induced by 1 mM IPTG for 16 hr at 25°C. The harvested cells were lysed by sonication and the supernatant was purified by nickel-NTA affinity chromatography. RAS proteins were subjected to thrombin cleavage, and further purified by Superdex 75 size exclusion chromatography (GE healthcare). Selective isotope labeling of {uniform (U)- [^{2}H], Ileδ1-[^{13}C^{1}H$_3$]} RAS was performed as described (Tugarinov et al., 2003). All RAS mutants were generated according to the QuikChange method (Agilent technologies).

In Vitro NMR Experiments

The resonance assignments of RAS were transferred from a previous study (Mazhab-Jafari et al., 2015). Each *in vitro* experiment was performed at 37°C in modified Hanks Balanced Salt Solution (HBSS: 30 mM HEPES-KOH (pH 7.2), 137 mM NaCl, 5.4 mM KCl, 0.25 mM Na_2HPO_4, 0.44 mM KH_2PO_4, 4.2 mM $NaHCO_3$, 1% w/v D-glucose 5 mM $MgCl_2$). *In vitro* GTP hydrolysis rate (k_{hy}) and GDP-GTP exchange rate (k_{ex}) were examined by recording the ^{1}H-^{13}C HSQC spectra of GTP-loaded RAS or RAS in the presence of 2-fold excess of GTPγS, respectively. Experiments using the GTP regeneration system also contained 10 munit /mL acetate kinase (AcK) and 10 mM acetyl phosphate (AcP) (Sigma Aldrich), 2-fold excess of GTP. The time-course of Ile21 signal intensity ratio was fitted to the Equation 1 for calculating the k_{hy} and k_{ex} values simultaneously.

$$[RAS_{GTP}]_t = \frac{\left([RAS_{GTP}]_0 + [RAS_{GDP}]_0\right)k_{ex}}{k_{hy}+k_{ex}} + \frac{[RAS_{GTP}]_0 k_{hy} - [RAS_{GDP}]_0 k_{ex}}{k_{hy}+k_{ex}} exp\left(-\left(k_{hy}+k_{ex}\right)t\right) \quad \text{(Equation 1)}$$

Where $[RAS_{GTP}]_x$ and $[RAS_{GDP}]_x$ denote the concentration of RAS in GTP or GDP-bound form, respectively, at the time x. The standard deviations of nonlinear fitting of the experiments are calculated by GraphPad Prism 8. The abundance of GTP in the NMR sample containing GTP regeneration system was estimated from the signal intensity of GTP β-phosphate obtained by time-resolved ^{31}P NMR spectrum.

Preparation of Cells for In-Cell NMR Measurements

GTP-loaded {U- [^{2}H], Ileδ1-[^{13}C^{1}H$_3$]} RAS was introduced into HeLa S3 cells using the SLO protocol as described previously (Ogino et al., 2009). The cells were subjected to density gradient centrifugation using 20% Percoll (GE Healthcare), for the removal of dead cells. The populations of the RAS-introduced cells and the dead cells were analyzed by a CytoFLEX flow cytometer (Beckman Coulter), as described previously (Ogino et al., 2009).

In-Cell NMR Measurement Using the Bioreactor System

All in-cell NMR experiments were performed at 37°C using an Avance III 800 spectrometer equipped with a cryogenic probe (Bruker Biospin). The RAS-containing cells (3×10^{7}) were encapsulated within 8% Mebiol gel within a 5 mm Shigemi NMR tube, and perfused with DMEM at a flow rate of 3 mL/h, as described previously (Kubo et al., 2013). ^{1}H-^{13}C SOFAST-HMQC spectra (Schanda et al., 2005) of the RAS-containing cells were acquired for every 30 min. The intracellular GTP-bound fraction of RAS was determined based on the signal intensities of δ1 methyl of Ile 21 as described above, and the intracellular k_{hy} and k_{ex} were measured by fitting the time-dependent decay of fGTPs of RAS to the Equation 1. The standard deviations of nonlinear fitting of the experiments are calculated by Graphpad Prism 8.

Preparation of Cell Lysates

Cell lysates (referred to as whole lysates) were prepared from HeLa S3 cells in suspended culture by sonication and stocked in −80°C freezer before the experiments. The lysate supernatants were prepared by centrifugation (15000 x g for 30 min). To prepare the heat-inactivated lysate, the supernatants were boiled 95°C 5 min, and aggregated debris were cleared by centrifugation (15000 x g for 30 min). To fractionate the lysate by molecular size, lysate supernatants are applied to Amicon Ultra 4 filters (Merck Millipore) with MWCO (100 kDa, 50 kDa, 30 kDa, 3 kDa) and the solution filtered through the membranes were added to NMR samples.

QUANTIFICATION AND STATISTICAL ANALYSIS

Bar graphs display value ± standard deviation from fitting errors calculated by nonlinear fitting of the experiments using GraphPad Prism 8 as described in the Method Details. Statistical methods were not utilized in analysis of the significance of data in this study.